Localization of the Antimitotic Peptide and Depsipeptide Binding Site on β-Tubulin[†]

Arpita Mitra[‡,§] and David Sept*[,§,||]

Departments of Chemical Engineering and Biomedical Engineering and Center for Computational Biology, Washington University, St. Louis, Missouri 63130

Received June 17, 2004; Revised Manuscript Received September 1, 2004

ABSTRACT: Several naturally occurring peptides and depsipeptides which include the cryptophycins, dolastatin 10, hemiasterlin, and phomopsin A have been found to be potent antimitotic agents, causing cell death at picomolar or low nanomolar concentrations. These compounds inhibit microtubule growth, modulate the dynamics of microtubules, and induce the self-association of tubulin dimers into single-walled rings and spirals. These peptides exhibit mutual competitive inhibition in binding to β-tubulin, while noncompetitively inhibiting the binding of vinblastine and vincristine to β-tubulin. Despite the abundance of biochemical information, the details of their molecular interactions with tubulin are not known. In this study, using a combination of molecular dynamics simulations and molecular docking studies, a common binding site for cryptophycin 1, cryptophycin 52, dolastatin 10, hemiasterlin, and phomopsin A on β-tubulin has been identified. Application of these same methods to α-tubulin indicated no interaction between α-tubulin and any of the peptides. On the basis of the docking results, a model for the mechanism of microtubule disruption and formation of aberrant nonmicrotubule structures is proposed. Both the active site and mechanism of microtubule depolymerization predictions are in good agreement with experimental findings.

Tubulin, the structural subunit of microtubules, was first identified as the "colchicine-binding protein" by Borisy and Taylor in 1967, and the ability of colchicine to block cells in the prometaphase−metaphase stage of mitosis was a critical step in the development of antimitotic drugs (*1*). Since then, three major classes of tubulin-binding drugs have been identified: (1) the colchicine-site binding agents, (2) the vinca domain inhibitors, which block microtubule growth and destabilize microtubules, and (3) the family of taxanes and epothilone inhibitors which stabilize microtubules. Among the various vinca domain inhibitors, of primary interest are the naturally occurring peptides and depsipeptides which bind in the peptide site of the vinca domain (*2*) and noncompetitively inhibit the binding of vinblastine and vincristine to β-tubulin, while stabilizing the colchicine binding activity of tubulin against time-dependent decay. Isolated from a diverse group of organisms, these antimitotic agents include the cryptophycins, obtained from the cyanobacterium *Nostoc* sp., the dolastatins, isolated from sea hare *Dolabella auricularia*, the hemiasterlins, isolated from the South African sponge *Hemiasterella minor*, and the phomopsins, produced by *Phomopsis leptostomiformis*. These inhibitors have been found to block cells in the G_2/M phase of the cell cycle at picomolar or low nanomolar concentrations and are highly cytotoxic to mammalian cells (for reviews, see refs *3* and *4*). These compounds modulate dynamic instability of cellular microtubules, disrupt spindle microtubules, inhibit microtubule assembly, and induce the self-association of tubulin dimers into single-protofilament rings and spirals. Additionally, all these peptides inhibit tubulin-dependent GTP[1] hydrolysis (*2*, *5*) as well as nucleotide exchange on β-tubulin (*2*, *6*, *7*) and, as a consequence, inhibit tubulin assembly. In murine xenograph models, these inhibitors show excellent antitumor activity against mammary, colon, and pancreatic adenocarcinomas (*8*). Except for dolastatin 10, all these compounds are weakly transported by P-glycoprotein and, thus, retain activity in cells exhibiting a multidrug resistant phenotype (*9*−*11*). Currently, all these drugs are undergoing clinical evaluation for cancer chemotherapy; therefore, it will be extremely valuable to have detailed knowledge of the structural basis of the interaction of these inhibitors with tubulin.

Extensive biochemical work has demonstrated that these peptides bind in the vicinity of the vinca binding site because of their inhibitory effects on binding of vincristine and vinblastine to tubulin (*2*, *5*, *6*, *12*, *13*). From experimental binding assays, it was observed that these compounds exhibit competitive inhibition of binding; namely, phomopsin A (*4*), cryptophycin 1 (*5*), and hemiasterlin (*12*) competitively inhibit the binding of dolastatin 10 to β-tubulin. On the other hand, cryptophycin 1 (*5*, *6*) and hemiasterlin (*12*) noncompetitively inhibit the binding of vinblastine to β-tubulin, while phomopsin A noncompetitively inhibits the binding of

[†] This research was supported by a grant from the Whitaker Foundation to D.S.

* To whom correspondence should be addressed. E-mail: dsept@biomed.wustl.edu.

[‡] Department of Chemical Engineering.

[§] Center for Computational Biology.

[||] Department of Biomedical Engineering.

[1] Abbreviations: GDP, guanosine 5′-diphosphate; GTP, guanosine 5′-triphosphate; Dov, dolavaline; Dil, dolaisoleucine; Dap, dolaproline; Doe, dolaphenine; rmsd, root-mean-square deviation.

10.1021/bi0487387 CCC: $27.50
Published on Web 10/16/2004

vincristine to β-tubulin (*2*). Each of these antimitotic agents destabilizes and depolymerizes microtubules, resulting in the formation of aberrant nonmicrotubule rings and oligomers. The phomopsin A−tubulin complex is observed to form 40 nm rings and spirals (*14*); cryptophycin 1−tubulin rings have a mean diameter of 24 nm, and are comprised of eight tubulin dimers (*15*), while the cryptophycin 52−tubulin rings are composed of nine $\alpha\beta$-tubulin dimers, having an outer diameter of 28 nm (*16*). Hemiasterlin−tubulin and dolastatin−tubulin rings are 45 nm in diameter, and both contain 14 tubulin dimers (*12*, *17*). The binding kinetics, for these vinca domain peptides, yields a biphasic Scatchard plot (*18*, *19*) resulting from the drug binding to a single high-affinity site followed by aggregation of the drug−tubulin complex (*20*).

Despite the wealth of available biochemical data, the details of the molecular interactions of these peptides with tubulin are not known. In this work, using a combination of molecular dynamics simulations and molecular docking, a common binding site for cryptophycin 1, cryptophycin 52, dolastatin 10, hemiasterlin, and phomopsin A on β-tubulin has been identified. On the basis of these results, a model for the mechanism of microtubule disruption and formation of aberrant nonmicrotubule structures is proposed.

MATERIALS AND METHODS

The ligands, namely, cryptophycin 1, cryptophycin 52, dolastatin 10, hemiasterlin, and phomopsin A (structures in Figure 1), were constructed as all-atom entities, energy-minimized using the Tripos force field, and assigned partial atomic charges based on the Gasteiger−Marsili method, all using the molecular docking program Sybyl, version 6.8 (Tripos Inc., St. Louis, MO).

The coordinates of bovine β-tubulin (with exchangeable-site GDP) were obtained from the Protein Data Bank (PDB entry 1JFF). Since the nucleotide present on the β-subunit of the tubulin dimer is more likely to be GTP, the diphosphate was converted to a triphosphate. Using the molecular dynamics package NAMD (*21*), simulations of the resulting bovine β-tubulin−GTP complex were performed at 300 K using an NPT ensemble with the CHARMM27 force field and explicit solvent (TIP3P water). The molecular dynamics simulations were comprised of energy minimization, followed by heating to 300 K at intervals of 75 K, equilibration for 500 ps, and finally the 2.5 ns production run. Representative conformations of the β-tubulin−GTP complex were extracted every 500 ps from the molecular dynamics trajectory for use in the AutoDock 3.0 (*22*) docking simulations. Since during the molecular docking runs the macromolecule structure was kept rigid, using multiple snapshots of the macromolecule allowed sampling of the side chain and backbone conformations and thereby captured some flexibility of the protein. For the multiple macromolecule structures obtained from the molecular dynamic simulation, the root-mean-square deviation (rmsd) fit based on backbone atoms was within 1.8 Å, which is comparable to the rmsd fit based on backbone atoms between the β-tubulin monomer structures obtained by electron microscopy (PDB entry 1JFF) and X-ray diffraction (PDB entry 1SA0).

Having obtained the macromolecule (i.e., β-tubulin−GTP complex) and ligand (i.e., peptide) structures, we carried out

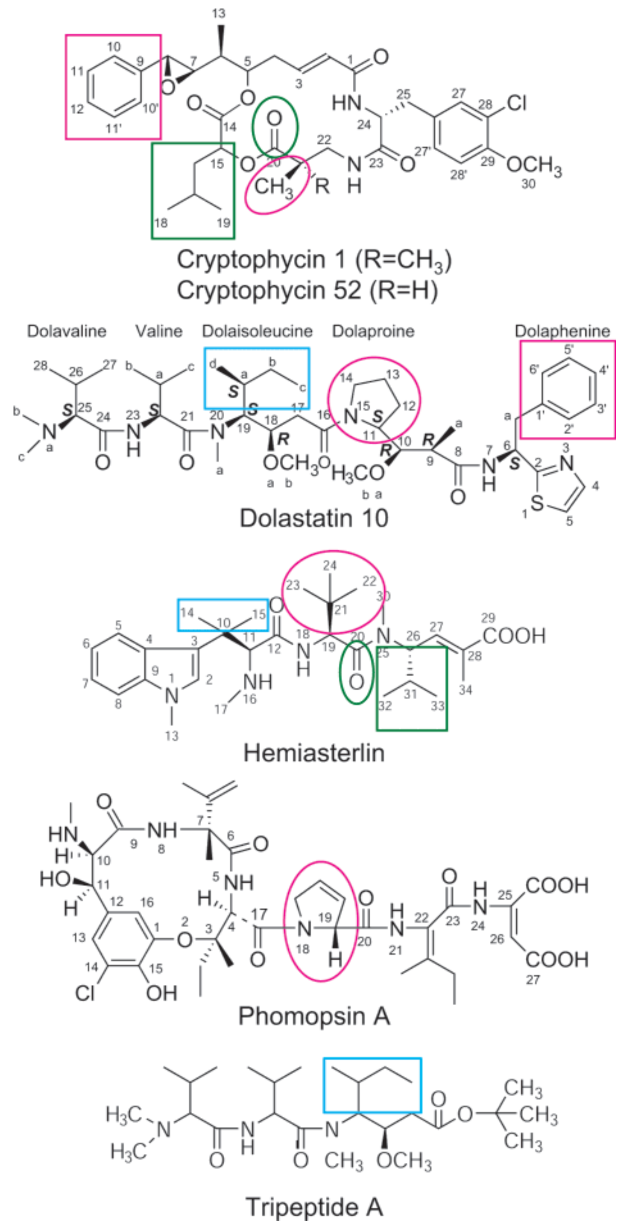

FIGURE 1: Structures of cryptophycin 1, cryptophycin 52 (numbering of cryptophycins as given for arenastatin A in ref *32*), dolastatin 10 (numbering as in ref *33*), hemiasterlin (numbering as in ref *34*), phomopsin A (numbering as in ref *35*), and tripeptide A (*2*). Boxed regions represent areas of common overlap identified through these docking studies.

flexible docking of the peptides over the entire macromolecule using a grid spacing of 0.375 Å. For each β-tubulin−GTP conformation obtained from the molecular dynamics trajectory, 30 docking runs were performed using the adapted Lamarckian genetic algorithm in AutoDock 3.0. The resulting structures were all clustered on the basis of an rmsd of 2.5 Å from the lowest docked energy conformation of the ligand. The site of the largest cluster having the lowest energy was selected as the active site of the ligand on the surface of the protein. Subsequently, a focused grid with 0.2 Å spacing was positioned on the binding site, to investigate the binding interactions in greater detail, and the flexible docking simulations were repeated with 30 runs per macromolecule conformation, followed by cluster analysis of the results using an rmsd of 1 Å. Table 1 shows the total number of clusters as well as the sizes of the top two clusters. The

Table 1: Total Number of Clusters and Top Cluster Sizes Resulting from 150 Docking Runs with Wild-Type α- and β-Tubulin as Well as the Ser172Ala β-Tubulin Mutant[a]

compound	target	no. of clusters	largest cluster	second cluster
CR1	WT β-tubulin	36	33	13
CR52	WT β-tubulin	24	30	18
DOL	WT β-tubulin	42	42	19
HEM	WT β-tubulin	27	35	17
PMA	WT β-tubulin	13	62	27
CR1	WT α-tubulin	75	19	10
CR52	WT α-tubulin	76	10	9
DOL	WT α-tubulin	92	10	5
HEM	WT α-tubulin	69	6	6
PMA	WT α-tubulin	53	18	14
CR1	Ser172Ala β-tubulin	63	12	10
CR52	Ser172Ala β-tubulin	55	16	11
DOL	Ser172Ala β-tubulin	91	9	6
HEM	Ser172Ala β-tubulin	48	23	15
PMA	Ser172Ala β-tubulin	35	26	18

[a] Note that for WT α-tubulin and the Ser172Ala mutant, the number of clusters increases and the clusters that do form are not at our identified binding site.

predicted binding affinity (K_d) was calculated using the binding free energy of the most stable complex among the various macromolecule conformations.

RESULTS

From docking the cryptophycins, dolastatin 10, hemiasterlin, and phomopsin A to multiple bovine β-tubulin conformations, a consensus high-affinity active site comprised of residues Ser172, Lys174, Val175, Asp177, Asn204, Glu205, Tyr208, Asp209, Phe212, Pro220, and Tyr222 was identified (see Figure 2). The active site had a cluster size of >20% of the total number of runs (see Table 1). Despite being structurally diverse, these antimitotic agents bind at the same active site, corroborating experimental data which show that the compounds competitively inhibit each other (*4*, *7*, *9*). This diversity of structures makes it very difficult to identify a common binding modality between these various inhibitors. However, we observed that all these peptides are largely hydrophobic and interact with β-tubulin to minimize the exposed hydrophobic surface area. These hydrophobic interactions result in a considerable lowering of the enthalpic contribution of the binding free energy. The presence of the methyl groups in the peptides reduces the potential number of hydrogen bonds that can be formed upon binding, but these groups also lower the desolvation penalty, making binding more favorable. Table 2 lists the predicted binding affinities calculated using the binding free energy of the most stable complex among the various macromolecule conformations obtained from AutoDock 3.0 along with the experimental binding affinities of these compounds with β-tubulin. The estimated error in the binding free energy predictions from AutoDock 3.0 can be as high as 2 kcal/mol; however, by docking the peptides to multiple β-tubulin structures taken from the molecular dynamics simulation trajectory, we achieved much better agreement with experimental values. Although the individual binding affinities do not match exactly, the values are very close and the relative ordering of the inhibitors is correct.

Having observed high-affinity binding of the peptides to β-tubulin, we repeated as a negative control the entire procedure of molecular dynamics simulations and molecular docking with α-tubulin. Despite the high degree of homology between α- and β-tubulin, none of the vinca domain peptides studied here docked with any specificity to α-tubulin. In the absence of consensus binding site(s), AutoDock 3.0 tends to the dock the ligands nonspecifically over the surface of the macromolecule. From the docking simulations, it was observed that the peptides were distributed over the α-tubulin surface so that no significant clusters were formed (Table 1). This result was interpreted as an indication of no interaction between these inhibitors and α-tubulin.

Several different β-tubulin isotypes and mutations exhibit resistance to the vinca domain drugs. A particular example is the Ser172 to Ala point mutation, observed in an ovarian carcinoma cell line (1A9), which confers resistance to a hemiasterlin analogue, HTI-286, and to vinca alkaloids (*23*). To investigate the effect of this mutation, Ser172 was computationally mutated to Ala and molecular dynamics simulations of the mutant followed by docking studies were performed. Our results indicate that this point mutation eliminates high-affinity binding at the active site identified in the wild-type protein.

Another interesting example of resistance to the vinca site drugs is the noninhibition of assembly of purified *Saccharomyces cerevisiae* tubulin by cryptophycin 1 and vinblastine at 2-fold molar excesses over tubulin (*24*). We propose that this may be due to polar residues, Thr175 and Gln212, forming the binding pocket in *S. cerevisiae* β-tubulin, as opposed to the hydrophobic residues, Val175 and Phe212, found in bovine β-tubulin. Both these examples lend support to the proposed location of the predicted binding pocket on bovine β-tubulin.

DISCUSSION

In this study, using a combination of molecular dynamics simulations and computational docking, a single high-affinity binding site on β-tubulin for five microtubule inhibitors (viz. cryptophycin 1, cryptophycin 52, dolastatin 10, hemiasterlin, and phomopsin A) has been identified. This binding pocket is adjacent to the exchangeable GTP site on β-tubulin and is composed primarily of residues Ser172, Lys174, Val175, Asp177, Asn204, Glu205, Tyr208, Asp209, Phe212, Pro220, and Tyr222.

Obtaining the structures of these peptides bound to β-tubulin allows one to evaluate the predictions in terms of existing experimental data. These peptides have been noted to inhibit nucleotide exchange and the hydrolysis of GTP (*2*, *5*−*7*). A straightforward explanation for this inhibition is that binding of these inhibitors is concomitant with oligomerization; however, on the basis of the proximity of the binding site to the nucleotide, there is the possibility that these peptides directly impede nucleotide exchange and/or hydrolysis. Some support for the latter comes from the docking results which show tripeptide A, which does not inhibit nucleotide exchange (*2*), binds ∼6 Å from the nucleotide (data not shown), while both dolastatin 10 and hemiasterlin bind closer, within 3.5 Å of GTP. The interaction of these compounds with residues that make up the nucleotide binding pocket could affect nucleotide exchange, but more experimental data are required. In addition to studies on nucleotide exchange, the sulfhydryl groups of

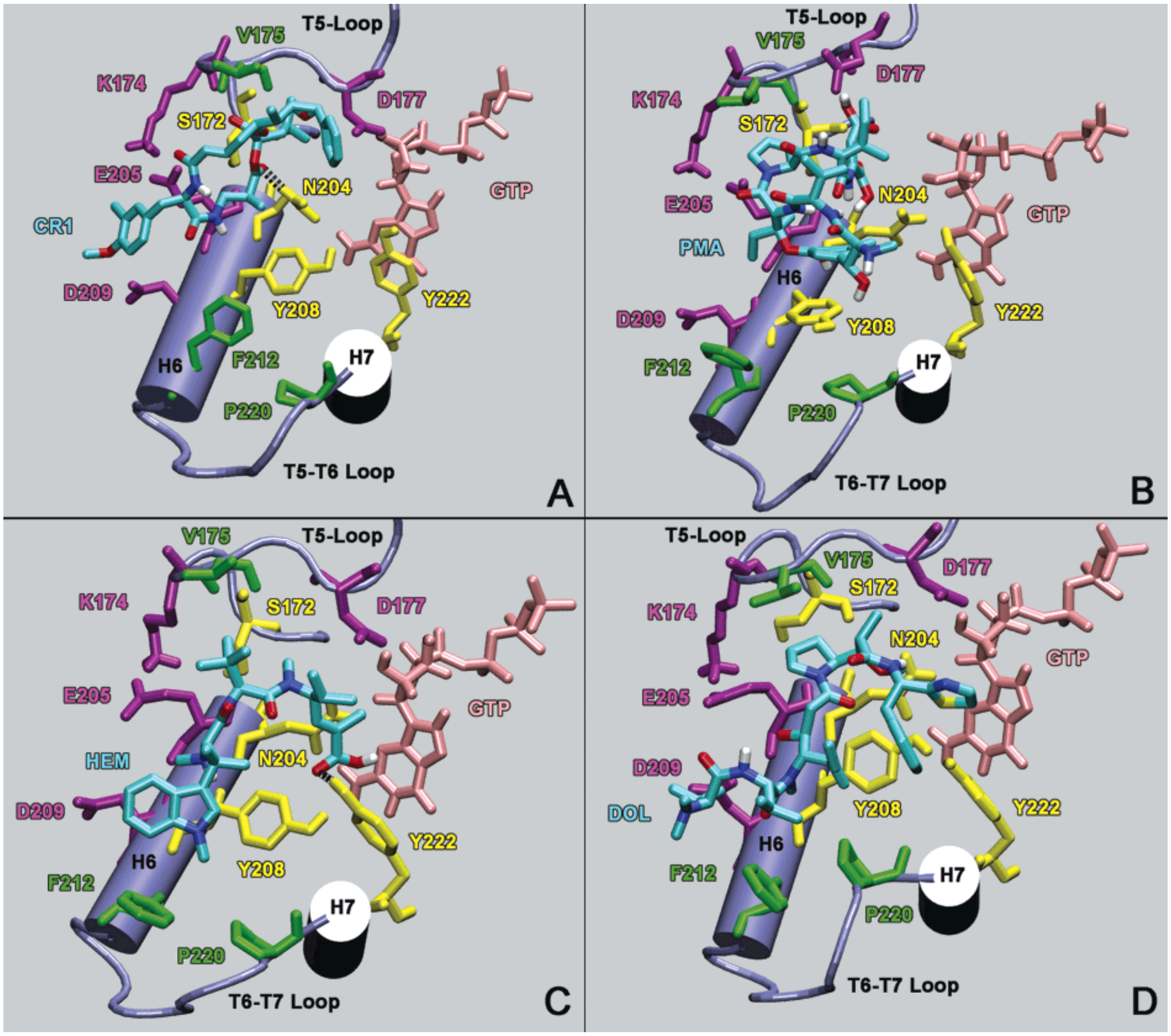

FIGURE 2: Representative structures of (A) cryptophycin 1, (B) phomopsin A, (C) hemiasterlin, and (D) dolastatin 10 bound to bovine β-tubulin as predicted by the docking simulations. The binding pocket is formed by hydrophobic residues (green), polar uncharged residues (yellow), and polar charged residues (magenta), all within 3 Å of the ligand. GTP is colored pink. Only polar hydrogens are shown for clarity. Hydrogen bonds are depicted as black springs. This figure was created using VMD (*36*).

Table 2: Predicted and Experimental Binding Affinities of Cryptophycin 1, Cryptophycin 52, Dolastatin 10, Hemiasterlin, and Phomopsin A with β-Tubulin

	predicted K_d (nM)	experimental K_d (nM)
cryptophycin 1	91	–
cryptophycin 52	57	47[a]
dolastatin 10	36	26[b]
hemiasterlin	7	–
phomopsin A	15	10[c]

[a] Taken from ref *11*. [b] Taken from ref *18*. [c] Taken from ref *19*.

β-tubulin have been used as targeted probes to investigate tubulin–antimitotic drug interactions (*25*). When tubulin is reacted with *N,N′*-ethylenebis(iodoacteamide), in the absence of exchangeable site guanine nucleotides, an intra-β-tubulin cross-link is formed between Cys12 and Cys211. The formation of this cross-link is inhibited completely by guanine nucleotides, as well as the vinca alkaloids, except vinblastine. Since these peptides prevent nucleotide exchange (*2*, *6*, *7*), they would as a direct consequence inhibit formation of the Cys12–Cys211 cross-link. However, given that these modified peptides are observed to bind to Asp209 and Phe212 of β-tubulin, the formation of this cross-link may be blocked even in the absence of a bound nucleotide. Further, the thiazole ring sulfur atom of dolastatin 10 is ∼9.5 Å from the sulfur atom of Cys12; hence, in the absence of a guanine nucleotide, cross-linking could occur between dolastatin 10 and Cys12. More experimental investigation will be required to resolve these issues.

Another experimental finding is the single nucleotide change in β-tubulin resulting in the Ser172 to Ala mutation which confers 8–20-fold resistance to a synthetic derivative of hemiasterlin, HTI-286, and 8–30-fold cross resistance to vinca alkaloids (*23*). On the basis of this result, the Ser172 to Ala mutation was computationally incorporated into the wild-type structure and the course of molecular dynamics and docking simulations was repeated. When docked to this mutant structure, the peptides no longer bound with high affinity at the active site identified in wild-type protein, but exhibited nonspecific interactions. This result indicates that a change from a polar residue (Ser) to a hydrophobic one (Ala) affects peptide binding, in addition to potential conformational or steric changes in the binding site.

Upon close examination of the residues forming the binding pocket, it is observed that these amino acids are

Biochemistry, Vol. 43, No. 44, 2004 13959

Table 3: Sequence Alignment of β-Tubulin Residues Pro171−Val180 and Cys201−Leu225 from Various Species with the Accession Numbers in Parentheses[a]

	171 ⋮ 201 ⋮
Sus scrofa (P02554)	P**S**P**KV**S**D**TVV....CID**NE**AL**YD**IC**F**RTLKLTT**P**T**Y**GDL
Homo sapiens (P05217)	P**S**P**KV**S**D**TVV....CID**NE**AL**YD**IC**F**RTLKLTT**P**T**Y**GDL
Leishmania mexicana (AAK31149)	P**S**P**RV**S**D**TVV.....CID**NE**AL**YD**IC**F**RTLKLTT**P**T**F**GDL
Plasmodium falciparum (P14643)	P**S**P**KV**S**D**TVV....VID**NE**AL**YD**IC**F**RTLKLTT**P**T**Y**GDL
Aspergillus nidulans (P10874)	P**S**P**KV**S**D**TVV....CLD**ND**AL**YD**IC**I**RTLKLSS**P**S**Y**GDL
S. cerevisiae (NP_116616)	P**S**P**KT**S**D**TVV...CID**NE**AL**YD**IC**Q**RTLKLNQ**P**S**Y**GDL
S. pombe (NP_596650)	P**A**P**KS**S**D**TVV...CID**NE**AL**SS**IF**A**NTLKIKS**P**S**Y**DDL

[a] The residues forming the peptide binding pocket on β-tubulin are shown in bold type.

conserved in vertebrate and protozoan β-tubulins, but not in fungal β-tubulins (see Table 3). Indeed, experimental results indicate that *Leishmania donovani* tubulin polymerization as well as promastigote growth is inhibited by hemiasterlin at micromolar concentrations (*26*), and the growth of *Plasmodium falciparum* microtubules during the schizont stage is arrested by dolastatin 10 and its synthetic derivatives (*27*); however, purified *S. cerevisiae* tubulin assembly is not affected by cryptophycin 1 at a 2-fold molar excess over tubulin (*24*), and phomopsin A is found not to bind appreciably to *Aspergillus nidulans*, *Schizosaccharomyces pombe*, and *S. cerevisiae* tubulins (*28*). On the basis of these results and the sequence alignment in Table 3, it appears that residues Thr175 and Gln212 of *S. cerevisiae* tubulin could impart resistance to the depsipeptides, presumably due to the loss of the hydrophobic contacts.

Previous efforts at gaining insight into the molecular interaction of these inhibitors with tubulin involved the modeling of cryptophycin 52 into a putative binding pocket formed by residues 205−215 of β-tubulin (*16*). This site was selected on the basis of the knowledge that cryptophycin bound to tubulin in the vicinity of the vinca binding site (*5*, *6*, *13*) and the vinblastine binding site was located between residues 175 and 213 of β-tubulin (*29*). Although the docking conformations of cryptophycin 52 postulated by Barbier and co-workers (*16*) and those determined by our docking simulations are in the same vicinity, the two predictions are fundamentally different. In our docking studies, no *a priori* assumption was made about the location of the active site; flexible docking of the peptides was performed over the entire macromolecule. As a result, the docking predictions in this study identify additional residues, Ser172−Asn204, Pro220, and Tyr222, as part of the binding pocket, and of these residues, Ser172 has been found to be an important residue as revealed by the Ser172 to Ala mutation which imparts resistance to a synthetic analogue of hemiasterlin (*23*).

Recently, using a benzophenone photoaffinity analogue of HTI-286, a synthetic derivative of hemiasterlin, researchers located a potential binding site on α-tubulin comprised of residues Ala314−Lys338 (*30*). These amino acid residues are located on strand S8, the S8−H10 loop, and helix H10 of α-tubulin. The binding site on β-tubulin predicted in this study is exactly at the interface with α-tubulin, and is located in a position such that when another dimer is added along the protofilament (see Figure 3), H10 of α-tubulin is in direct

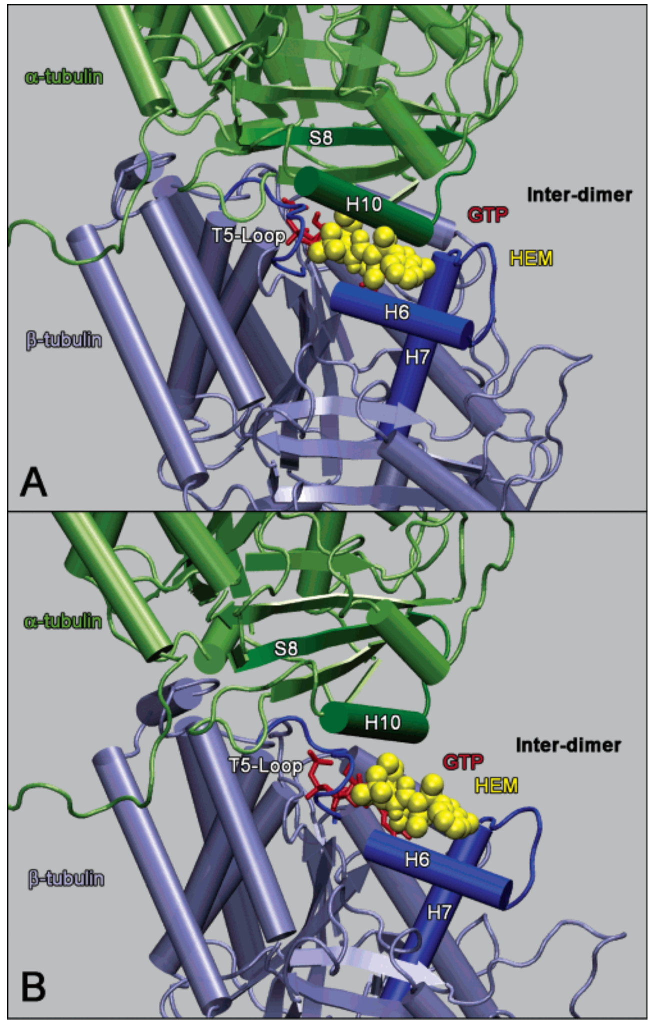

FIGURE 3: (A) Proximity of the photoaffinity cross-linking site on α-tubulin to our predicted binding site on β-tubulin. Note that helix H10 of α-tubulin is in direct contact with the peptides in the binding site. (B) A proposed curved conformation of α-tubulin that prevents these steric clashes. This figure was created using VMD (*36*).

contact with the bound peptide on β-tubulin. To create the photoaffinity analogue, the indole ring in hemiasterlin was replaced with benzophenone. The carbonyl oxygen in benzophenone is known to react preferentially with unreactive C−H bonds, including those in the side chains of Leu, Val, Lys, Arg, and Met (*31*). Although the photoaffinity analogue has not been modeled in this study, the docked hemiasterlin structure places C9 (see Figure 1) only ~2.5 Å from C_ϵ of Lys326 in α-tubulin. On the basis of this observation, the binding site appears to be in very good agreement with the photoaffinity cross-linking results.

The peptides and depsipeptides investigated in this study, despite being diverse in structure, are all comprised of modified hydrophobic residues derived from Val, Ile/Leu, and Pro. Hence, to identify a common binding modality among these inhibitors, it is instructive to compare their binding predictions with each other, based on their structures, orientations at the docked site, and their binding affinities for β-tubulin. The common regions of overlap between the various compounds are outlined in Figure 1, and the specific details are given below.

When hemiasterlin and dolastatin 10 are compared, it is noted that hemiasterlin is a linear tripeptide composed of modified hydrophobic residues derived from a Trp-Val-Ile motif while dolastatin 10 is a linear pentapeptide formed of Dov-Val-Dil-Dap-Doe motifs. From their sequences, hemiasterlin is seen to be similar to the first three residues of dolastatin 10, and the docking results in this study show that hemiasterlin overlaps the first four residues of dolastatin 10 in the peptide binding pocket, with the amino termini of both peptides oriented in the same direction. Upon observation of the binding orientation of hemiasterlin, the hydroxyl group of Tyr222 is found to hydrogen bond with the C29 carbonyl oxygen of hemiasterlin (Figure 2C). Further, on the basis of the structures of these two hydrophobic peptides and the docking predictions, it is observed that the aliphatic side chain of the Dil moiety of dolastatin 10 may exhibit overlap with the methyl groups of the Trp residue of hemiasterlin, while the aliphatic side chain of the Val residue of hemiasterlin probably overlaps the pyrrolidine ring of the Dap moiety of dolastatin 10 (see Figure 1). These results suggest that the Val, Ile, and Pro amino acid residues are possibly the structural elements forming the pharmacophore.

On evaluating dolastatin 10 and phomopsin A, researchers have observed that these peptides are very similar in their interactions with tubulin (*2*). Dolastatin 10 is a linear peptide composed of altered Val-Val-Ile-Pro-Phe motifs, while phomopsin A is a conjoined macrocyclic peptide formed of modified Phe-Val-Ile-Pro-Ile-Asp motifs. Therefore, these peptides are structurally similar, containing hydrophobic residues derived from Val, Ile, and Pro. On the basis of the docking results, it is observed that for both these peptides, the pyrrolidine ring of the modified Pro is oriented toward polar residue Ser172 (see Figure 2B,D) and forms a region of common overlap between these inhibitors as shown in Figure 1. Further, from the binding orientation of phomopsin A, it is noted that the phenyl ring of its Tyr moiety shows ring stacking with the phenyl ring of Tyr208 (see Figure 2B).

Upon analysis of the functional behavior of dolastatin 10 and tripeptide A, a carboxyl-protected synthetic precursor of dolastatin 10 (structure in Figure 1), it has been noted that tripeptide A inhibits tubulin polymerization and tubulin-dependent GTP hydrolysis, but is unable to inhibit nucleotide exchange on tubulin (*2*). Tripeptide A contains the first three amino-terminal residues of dolastatin 10. From the docking predictions, it is observed that tripeptide A binds to β-tubulin with a binding free energy ~1.65 kcal/mol lower than that of dolastatin 10. Further, the docking orientation of tripeptide A is such that it is located ~6 Å from the E-site GTP (data not shown) and is similar to the orientation of the first three amino-terminal residues of dolastatin 10 in the peptide binding site (see Figure 2D). On the basis of the noninhibition of nucleotide exchange by tripeptide A (*2*), the suggestion that the Dap and Dae residues prevent access to the exchangeable nucleotide site is consistent with these docking predictions.

From docking of cryptophycin 1 (Figure 2A) and cryptophycin 52 (figure not shown) to β-tubulin, it is noted that these inhibitors bind with an identical orientation in the peptide binding site. The cryptophycins are macrocyclic depsipeptides containing modified Tyr, Val, and Leu residues. The docking results indicate that these compounds bind to β-tubulin in an orientation that is the opposite of that of dolastatin 10 and hemiasterlin. In other words, the carboxyl terminus of the cryptophycins is directed toward the amino termini of hemiasterlin and dolastatin 10. Further, upon comparison of the structures as well as the binding orientation of these depsipeptides with dolastatin 10, it is postulated that the phenyl ring (ring A) of cryptophycin overlaps with the phenyl ring of the Dap moiety of dolastatin 10, and could therefore have a function similar to that of the Dap residue in dolastatin 10, blocking access to the vinca and exchangeable nucleotide sites (see Figure 2A,D). Next, upon comparison of the bound structures of the cryptophycins with hemiasterlin, it is noted that overlap may exist between the C20 carbonyl groups of the Val moieties and the aliphatic side chains of the Val and Dil/Leu residues may show structural overlap (see Figure 2A,C). These predictions once again indicate that the Val and Ile/Leu residues may be the common elements forming the pharmacophore. Finally, the C20 carbonyl group of the altered Val residue, which may form a part of the pharmacophore, hydrogen bonds with the δ-amino group of Asn204 (see Figure 2A).

Apart from a structural evaluation of the peptides, it is instructive to compare the binding affinities obtained by performing multiple docking simulations. The advantage of using multiple β-tubulin structures for docking is that it allows sampling of the side chain and backbone conformations of tubulin and thereby captures some flexibility of the protein. Since the estimated error in the binding free energy calculations using AutoDock is $\leq$2 kcal/mol, only an order of magnitude estimate of the binding affinities can be obtained, and not their exact values. Despite this limitation, a fairly good agreement with experimental data is achieved for cryptophycin 52 (*11*), dolastatin 10 (*18*), and phomopsin A (*19*) as seen in Table 2. By coupling molecular dynamics simulations with molecular docking, we observe reasonable agreement with experimental data, in terms of both the active site predictions and the binding affinities. This clearly demonstrates the potential of the molecular docking program in effectively docking the inhibitors to tubulin without any prior knowledge of the binding site(s).

Since these docking results point to a single high-affinity binding pocket formed by loop T5, helix H6, the H6−H7 loop, and the N-terminal end of core helix 7, and also located at the "plus" end of the microtubule, this prediction can be used to develop a model for the mechanism of microtubule disruption and formation of single-walled rings and sheets. At the polymerizing microtubule end, the binding of the peptides to β-tubulin would induce a conformational change in the dimer, which has been observed experimentally with cryptophycin 52 binding to tubulin using circular dichroism spectroscopy (*13*). Further, the binding of these peptides at this site on β-tubulin would interfere with the addition of tubulin dimers at the end of the protofilaments in a vertical conformation due to steric clashes. As seen in Figure 3A, if another dimer is added in a straight protofilament conformation, helix H10 and strand S9 of α-tubulin would overlap with the peptides bound in the active site. To avoid these clashes, the added dimer would have to be deformed and/or reorient to adopt a curved conformation (Figure 3B), producing a "kink" at the interdimer interface. This in turn would disrupt the longitudinal contacts between the residues of helix H6 and the H6−H7 loop of β-tubulin and the residues of strand S8, helix H10, and strand S9 of α-tubulin, thereby weakening the interdimer interactions. Also, the curvature in the protofilaments would result in a loss of lateral interactions between protofilaments, ultimately leading to microtubule destabilization and disruption. The closure of the curved protofilaments would lead to the formation of rings with the inside of the protofilament forming the outside of the ring. This model is consistent with the experimentally obtained cryptophycin−tubulin ring structure analyzed by cryoelectron microscopy and image analysis (*15*). Additionally, the opening of the microtubule along the seam would result in sheet formation. The presence of these rings and sheets has been observed experimentally for cryptophycin 1 (*15*), cryptophycin 52 (*16*), phomopsin A (*14*), hemiasterlin, and dolastatin (*12*, *17*).

In summary, through the use of molecular modeling, a single high-affinity site on β-tubulin has been identified, and on the basis of this prediction, a model for the mechanism of microtubule disruption and formation of aberrant nonmicrotubule structures has been developed. It is hoped that the comparison of these various compounds and the identification of their common binding features will assist in and lead to the development of more effective peptide-based inhibitors. The molecular coordinates of the bound peptides are available upon request from the authors.

ACKNOWLEDGMENT

We thank Dan Sackett for many useful discussions and a critical reading of the manuscript.

SUPPORTING INFORMATION AVAILABLE

Stereo images of the docked structures shown in Figure 2 (Figures S1−S4). This material is available free of charge via the Internet at http://pubs.acs.org.

REFERENCES

1. Borisy, G. G., and Taylor, E. W. (1967) The mechanism of action of colchicine. Colchicine binding to sea urchin eggs and the mitotic apparatus, *J. Cell Biol. 34*, 535−548.
2. Bai, R. L., Pettit, G. R., and Hamel, E. (1990) Binding of dolastatin 10 to tubulin at a distinct site for peptide antimitotic agents near the exchangeable nucleotide and vinca alkaloid sites, *J. Biol. Chem. 265*, 17141−17149.
3. Hamel, E., and Covell, D. G. (2002) Antimitotic peptides and depsipeptides, *Curr. Med. Chem.: Anti-Cancer Agents 2*, 19−53.
4. Hamel, E. (2002) Interactions of antimitotic peptides and depsipeptides with tubulin, *Biopolymers 66*, 142−160.
5. Bai, R., Schwartz, R. E., Kepler, J. A., Pettit, G. R., and Hamel, E. (1996) Characterization of the interaction of cryptophycin 1 with tubulin: binding in the Vinca domain, competitive inhibition of dolastatin 10 binding, and an unusual aggregation reaction, *Cancer Res. 56*, 4398−4406.
6. Smith, C. D., and Zhang, X. (1996) Mechanism of action cryptophycin. Interaction with the Vinca alkaloid domain of tubulin, *J. Biol. Chem. 271*, 6192−6198.
7. Bai, R., Pettit, G. R., and Hamel, E. (1990) Dolastatin 10, a powerful cytostatic peptide derived from a marine animal. Inhibition of tubulin polymerization mediated through the vinca alkaloid binding domain, *Biochem. Pharmacol. 39*, 1941−1949.
8. Al-Awar, R. S., Ray, J. E., Schultz, R. M., Andis, S. L., Kennedy, J. H., Moore, R. E., Liang, J., Golakoti, T., Subbaraju, G. V., and Corbett, T. H. (2003) A convergent approach to cryptophycin 52 analogues: synthesis and biological evaluation of a novel series of fragment A epoxides and chlorohydrins, *J. Med. Chem. 46*, 2985−3007.
9. Smith, C. D., Zhang, X., Mooberry, S. L., Patterson, G. M., and Moore, R. E. (1994) Cryptophycin: a new antimicrotubule agent active against drug-resistant cells, *Cancer Res. 54*, 3779−3784.
10. Loganzo, F., Discafani, C. M., Annable, T., Beyer, C., Musto, S., Hari, M., Tan, X., Hardy, C., Hernandez, R., Baxter, M., Singanallore, T., Khafizova, G., Poruchynsky, M. S., Fojo, T., Nieman, J. A., Ayral-Kaloustian, S., Zask, A., Andersen, R. J., and Greenberger, L. M. (2003) HTI-286, a synthetic analogue of the tripeptide hemiasterlin, is a potent antimicrotubule agent that circumvents P-glycoprotein-mediated resistance in vitro and in vivo, *Cancer Res. 63*, 1838−1845.
11. Panda, D., DeLuca, K., Williams, D., Jordan, M. A., and Wilson, L. (1998) Antiproliferative mechanism of action of cryptophycin-52: kinetic stabilization of microtubule dynamics by high-affinity binding to microtubule ends, *Proc. Natl. Acad. Sci. U.S.A. 95*, 9313−9318.
12. Bai, R., Durso, N. A., Sackett, D. L., and Hamel, E. (1999) Interactions of the sponge-derived antimitotic tripeptide hemiasterlin with tubulin: comparison with dolastatin 10 and cryptophycin 1, *Biochemistry 38*, 14302−14310.
13. Panda, D., Ananthnarayan, V., Larson, G., Shih, C., Jordan, M. A., and Wilson, L. (2000) Interaction of the antitumor compound cryptophycin-52 with tubulin, *Biochemistry 39*, 14121−14127.
14. Tonsing, E. M., Steyn, P. S., Osborn, M., and Weber, K. (1984) Phomopsin A, the causative agent of lupinosis, interacts with microtubules in vivo and in vitro, *Eur. J. Cell Biol. 35*, 156−164.
15. Watts, N. R., Cheng, N., West, W., Steven, A. C., and Sackett, D. L. (2002) The cryptophycin-tubulin ring structure indicates two points of curvature in the tubulin dimer, *Biochemistry 41*, 12662−12669.
16. Barbier, P., Gregoire, C., Devred, F., Sarrazin, M., and Peyrot, V. (2001) In vitro effect of cryptophycin 52 on microtubule assembly and tubulin: molecular modeling of the mechanism of action of a new antimitotic drug, *Biochemistry 40*, 13510−13519.
17. Boukari, H., Nossal, R., and Sackett, D. L. (2003) Stability of drug-induced tubulin rings by fluorescence correlation spectroscopy, *Biochemistry 42*, 1292−1300.
18. Bai, R., Taylor, G. F., Schmidt, J. M., Williams, M. D., Kepler, J. A., Pettit, G. R., and Hamel, E. (1995) Interaction of dolastatin 10 with tubulin: induction of aggregation and binding and dissociation reactions, *Mol. Pharmacol. 47*, 965−976.
19. Li, Y., Kobayashi, H., Tokiwa, Y., Hashimoto, Y., and Iwasaki, S. (1992) Interaction of phomopsin A with porcine brain tubulin. Inhibition of tubulin polymerization and binding at a rhizoxin binding site, *Biochem. Pharmacol. 43*, 219−224.
20. Timasheff, S. N., Andreu, J. M., and Na, G. C. (1991) Physical and spectroscopic methods for the evaluation of the interactions of antimitotic agents with tubulin, *Pharmacol. Ther. 52*, 191−210.
21. Kale, L., Skeel, R., Bhandarkar, M., Brunner, R., Gursoy, A., Krawetz, N., Phillips, J., Shinozaki, A., Varadarajan, K., and Schulten, K. (1999) NAMD2: Greater scalability for parallel molecular dynamics, *J. Comput. Phys. 151*, 283−312.
22. Morris, G. M., Goodsell, D. S., Halliday, R. S., Huey, R., Hart, W. E., Belew, R. K., and Olson, A. J. (1998) Automated Docking Using a Lamarckian Genetic Algorithm and Empirical Binding Free Energy Function, *J. Comput. Chem. 19*, 1639−1662.
23. Poruchynsky, M. S., Kim, J.-H., Nogales, E., Annable, T., Loganzo, F., Greenberger, L. M., Sackett, D. L., and Fojo, T. (2004) Tumor cells resistant to a microtubule-depolymerizing hemiasterlin analog, HTI-286, have mutations in α- or β-tubulin and increased microtubule stability, *Biochemistry* (in press).
24. Bode, C. J., Gupta, M. L., Jr., Reiff, E. A., Suprenant, K. A., Georg, G. I., and Himes, R. H. (2002) Epothilone and paclitaxel: unexpected differences in promoting the assembly and stabilization of yeast microtubules, *Biochemistry 41*, 3870−3874.
25. Luduena, R. F., and Roach, M. C. (1991) Tubulin sulfhydryl groups as probes and targets for antimitotic and antimicrotubule agents, *Pharmacol. Ther. 49*, 133−152.
26. Havens, C. G., Bryant, N., Asher, L., Lamoreaux, L., Perfetto, S., Brendle, J. J., and Werbovetz, K. A. (2000) Cellular effects of leishmanial tubulin inhibitors on *L. donovani*, *Mol. Biochem. Parasitol. 110*, 223−236.
27. Fennell, B. J., Carolan, S., Pettit, G. R., and Bell, A. (2003) Effects of the antimitotic natural product dolastatin 10, and related peptides, on the human malarial parasite *Plasmodium falciparum*, *J. Antimicrob. Chemother. 51*, 833−841.
28. Li, Y., Kobayashi, H., Hashimoto, Y., and Iwasaki, S. (1992) Binding selectivity of rhizoxin, phomopsin A, vinblastine and ansamitocin P-3 to fungal tubulins: differential interactions of

these antimitotic agents with brain and fungal tubulins, *Biochem. Biophys. Res. Commun. 187*, 722−729.
29. Rai, S. S., and Wolff, J. (1996) Localization of the vinblastine-binding site on β-tubulin, *J. Biol. Chem. 271*, 14707−14711.
30. Nunes, M., Kaplan, J., Wooters, J., Minnick, A. A., May, M. K., Shi, C., Musto, S., Beyer, C., Krishnamurthy, G., Qiu, Y., Loganzo, F., Ayral-Kaloustian, S., Zask, A., and Greenburger, L. M. (2004) A photoaffinity analog of the tripeptide hemiasterlin labels α-tubulin within residues 314−338, *Proc. Am. Assoc. Cancer Res. 45*, A2483.
31. Dorman, G., and Prestwich, G. D. (1994) Benzophenone photophores in biochemistry, *Biochemistry 33*, 5661−5673.
32. Kobayashi, M., Kurosu, M., Ohyabu, N., Wang, W., Fujii, S., and Kitagawa, I. (1994) The absolute stereostructure of arenastatin A, a potent cytotoxic depsipeptide from the Okinawan marine sponge, *Dysidea arenaria*, *Chem. Pharm. Bull. 42*, 2196−2198.
33. Petit, G. R., Kamano, Y., Herald, C. L., Tuinman, A. A., Boettner, F. E., Kizu, H., Schmidt, J. M., Baczynskyj, L., Tomer, K. B., and Bontems, R. J. (1987) The isolate and structure of a remarkable marine animal antineoplastic constituent: dolastatin 10, *J. Am. Chem. Soc. 109*, 6883−6885.
34. Coleman, J. E., Desilva, E. D., Kong, F. M., Andersen, R. J., and Allen, T. M. (1995) Cytotoxic Peptides from the Marine Sponge *Cymbastela* sp, *Tetrahedron 51*, 10653−10662.
35. Mackay, M. F., Van Donkelaar, A., and Culvenor, C. C. J. (1986) The X-ray structure of Phomopsin A, a Hexapeptide Mycotoxin, *J. Chem. Soc.*, *Chem. Commun.*, 1219−1221.
36. Humphrey, W., Dalke, A., and Schulten, K. (1996) VMD: Visual molecular dynamics, *J. Mol. Graphics 14*, 33−38.

BI0487387